Complexation of trivalent lanthanides (Eu) and actinides (Cm) with aqueous phosphates at elevated temperatures

Jordan, N.; Demnitz, M.; Lösch, H.; Starke, S.; Brendler, V.; Huittinen, N.;

Originally published:

June 2018

Inorganic Chemistry 57(2018)12, 7915-7024

DOI: https://doi.org/10.1021/acs.inorgchem.8b00647

Complexation of trivalent lanthanides (Eu) and actinides (Cm) with aqueous phosphates at elevated temperatures

N. Jordan[1,*], M. Demnitz[1], H. Lösch[1], S. Starke[2], V. Brendler,[1] N. Huittinen[1,*]

[1]*Helmholtz-Zentrum Dresden - Rossendorf, Institute of Resource Ecology, Bautzner Landstraße 400, 01328 Dresden, Germany*

[2]*Helmholtz-Zentrum Dresden – Rossendorf, Computational Science Group (FWCC), Department of Information Services and Computing (FWC), Bautzner Landstraße 400, 01328 Dresden, Germany*

**Corresponding author:*

Phone: +49 351 260 2148, E-mail: n.jordan@hzdr.de

Phone: +49 351 260 2148, E-mail: n.huittinen@hzdr.de

ABSTRACT

In this study, the complexation of Eu(III) and Cm(III) with aqueous phosphates was investigated using laser-induced luminescence spectroscopy. Experiments at 25 °C and different ionic strengths (0.6 to 3.1 $mol \cdot L^{-1}$ $NaClO_4$) established the formation of $EuH_2PO_4^{2+}$ and $CmH_2PO_4^{2+}$. From the conditional stability constants, the respective values at infinite dilution as well as the $\varepsilon(Me(H_2PO_4)^{2+};ClO_4^-)$ (Me = Eu or Cm) ion interaction coefficients (using the specific ion interaction theory - SIT) were derived. Further experiments (at constant ionic strength of 1.1 $mol \cdot L^{-1}$) showed, that upon increasing the temperature (25-80 °C), the formation of both $EuH_2PO_4^{2+}$ and $CmH_2PO_4^{2+}$ was favored. Using the van't Hoff equation, the enthalpy $\Delta_R H_m^0$ and entropy $\Delta_R S_m^0$ of these reactions were derived, corroborating an endothermic and entropy driven complexation process. This work contributes to a better understanding of the coordination chemistry of both trivalent actinides and lanthanides with phosphate ions.

Keywords

Complexation; Europium; Curium; Aqueous phosphate; Temperature; Luminescence spectroscopy

INTRODUCTION

Together with other parameters compiled in thermodynamic databases (TDB), such as fugacity of gaseous phases, enthalpy, entropy, heat capacity and Gibbs free energy, the reliability and internal consistency of solubility products ($K_{sp}°$ for amorphous and crystalline phases) and aqueous complexation constants (log β°) of potential environmental contaminants are important key parameters.

TDB find use in many applications such as underground disposals of chemotoxic waste, decontamination of polluted areas, hydrometallurgy, electrochemistry, corrosion science, and chemical engineering. Other relevant uses concern the safety assessments of future high-level radioactive waste (HLW) disposal sites and the optimization of technological processes to access critical raw materials such as Rare Earth Elements (REE). Thus, a detailed comprehension and generation of reliable data, describing the key mechanisms controlling the mobility of contaminants in the environment, is of great importance. Such mechanisms include adsorption, surface precipitation, ion exchange, incorporation, and redox reactions on mineral phases, formation and stability of colloids, various interactions with microorganisms as well as aqueous complexation by organic/inorganic ligands.

Raw material recovery involves optimization of technological processes used in the recovery process, making them more efficient, sustainable, and energy-saving. The development of innovative technologies for improving recovery and recycling critical raw materials from ore bodies during their mining from natural deposits, separation, processing, and finally recycling from secondary resources (called the value creation chain), is of paramount interest for the worldwide economy to safeguard a steady supply of raw materials. The modeling of flowsheets, graphically representing the variety of physico-chemical operations involved in the value creation chain, is highly depending on reliable TDB. Thermodynamic-based prediction is a cost-effective and time-saving approach, which allows increasing the economic efficiency and the environmental friendliness, as well as designing more effective extraction and recycling processes.

In the field of HLW disposal safety, the environmental fate of radionuclides (RNs) such as actinides and fission products disposed in underground nuclear waste repositories is of

major concern. Long term safety assessments of these disposal sites rely on the ability of geochemical models and TDB to forecast the mobility of RN over very long time periods.

One of several examples where relevant thermodynamic data is scarce or even completely missing is related to the complexation of lanthanides (with relevance to REE recovery) and actinides (with relevance to HLW disposal) with aqueous phosphates. Orthophosphate ions are ubiquitous in the environment and may originate from the natural decomposition of rocks and minerals (e.g. monazite or apatite), agricultural runoff, or from wastewater treatment plants. Solid phosphate monazites are one of the most important ore bodies for the recovery of REE (e.g. Kumari et al.[1]), while future monazite applications may involve their use as immobilization matrices for specific HLW streams.[2-4] The phosphate concentrations expected from respective mineral dissolution are difficult to estimate and depend on a variety of (geo)chemical boundary conditions. The more it is essential to identify relevant species sets for aqueous trivalent f-element phosphates and their stability regions. Another side effect is the potential to form secondary phases which again may significantly impact on REE and actinide mobility.

The situation concerning the complexation of Eu(III) with phosphate ions is quite unsatisfactory, although it has been used for decades as an analogue for other trivalent lanthanides and even trivalent actinides. In fact, there is not a single experimental log β value determined directly for aqueous europium phosphates. All the available data is based on extrapolation using linear free-energy relationships (LFER) from the work of Byrne et al.,[5] who studied only the complexation of Gd(III) and Ce(III) by phosphate ions at 25 °C by solvent extraction. Formation constants for $GdPO_4^0$, $GdHPO_4^+$, $Gd(HPO_4)_2^-$ and $GdH_2PO_4^{2+}$ were reported, while the presence of only $CePO_4^0$ was considered sufficient to explain the experimental data. As highlighted by Hummel et al.,[6] this surprising set of Gd species was selected solely on the basis that an acceptable fit of the experimental data could be obtained, with similar statistical errors for all four Gd complexes. Thus, without any independent spectroscopic proof of existence, the use of such a set of species in a LFER extrapolation should be done with caution.

For actinides such as americium and curium, Silva et al.[7] recommended a log β° value for $AmH_2PO_4^{2+}$ at 25 °C, based on the solvent extraction study of Rao et al.[8]. However, based on the same study, a value for $AmHPO_4^+$ could not be recommended by Silva et

al.,[7] as the stoichiometry of the dominant species ($AmHPO_4^+$ or $AmPO_4$) in neutral and weakly basic conditions was not unambiguously proven. Later on, Morgenstern[9] and Moll et al.[10] reported formation constants of $CmH_2PO_4^{2+}$ determined by means of laser spectroscopy at 25 °C, while that of $CmHPO_4^+$ was only reported by Moll et al.[10] No spectroscopic evidence for the formation of other species such as $MePO_4^0$ or $Me(HPO_4)_2^-$ (Me = Ln(III) or An(III)) is available in the literature. Consequently, a complete and reliable set of Ln(III)/An(III) phosphate species is currently still missing, as are respective complex formation constants. Furthermore, there are no studies dealing with the impact of elevated temperatures on An/Ln complexation with aqueous phosphates, despite the relevance of high temperatures in both REE leaching from monazites minerals and in the proximity of heat-generating HLW repositories.

Thus, the general purpose of this study was to close a critical gap of knowledge related to the coordination chemistry of both actinides and lanthanides with phosphate, and to derive complexation constants for spectroscopically identified species. Due to the challenging low solubility of Ln(III) and An(III) phosphate phases,[11-13] the experiments were performed at acidic pH (−log $[H^+]$ = 0.1) at 25 °C. The complexation of the lanthanide Eu(III) and the actinide Cm(III) with phosphate was investigated by means of laser induced luminescence spectroscopy. Indeed, such an advanced spectroscopic tool allows (i) *in situ* monitoring of the Ln/An speciation at micromolar concentrations and below, and simultaneously (ii) identifying the prevailing species as well as their stoichiometries. In order to keep the activity coefficients constant for the calculation of conditional stability constants, the ionic medium method was applied, which is based on the use of high concentrations of an inert background electrolyte (0.6 to 3.1 $mol \cdot L^{-1}$ $NaClO_4$). It enables the application of the specific ion interaction theory (SIT) to derive the complexation constant at infinite dilution (log β°) as well as the respective ion interaction coefficients (ε). Thermodynamic parameters such as the molal enthalpy of reaction ($\Delta_R H_m^0$) and the molal entropy of reaction ($\Delta_R S_m^0$) are required to describe the environmental fate of Ln(III) and An(III) at temperatures other than 25 °C. Such parameters were derived by investigating the impact of elevated temperature (25 to 80 °C) on the complexation reaction followed by using the linear van´t Hoff equation.

EXPERIMENTAL SECTION

Reagents

Solutions were prepared with high purity reagent grade materials without any further treatment. $EuCl_3 \cdot 6H_2O$ (Sigma - Aldrich, 99.99 % purity) was dissolved in $1 \cdot 10^{-3}$ mol·L^{-1} $HClO_4$ to obtain a europium stock solution having an initial concentration of $1 \cdot 10^{-3}$ mol·L^{-1}. For the curium experiments, a $1 \cdot 10^{-4}$ mol·L^{-1} ^{248}Cm stock solution in 0.1 mol·L^{-1} $HClO_4$ was used. Aliquots from these stock solutions were taken to obtain the desired Eu or Cm final concentrations. $NaClO_4 \cdot H_2O$ (Sigma-Aldrich, p.a., ACS reagent, ≥ 99.5 %) was taken as a background electrolyte. Ortho-Phosphoric acid (85 % from Merck/Roth) was used as a source of phosphate ions.

pH measurements

At ionic strengths higher than 0.1 mol·L^{-1}, the pH measured in solutions (pH_{exp}) is an operational apparent value.[14-17] It can be related to the molar H^+ concentration as given in Equation 1:

$$-\log [H^+] = pH_{exp} + A_c \quad (1)$$

The liquid junction potential, which depends on the electrolyte concentration, differs for saline solutions and dilute buffer solutions (used for the calibration of the pH electrode). This variation together with the individual activity coefficient $\gamma_{H+,}$ are included in the term A_c, which depends exclusively on the concentration and composition of the solutions.[14-17]

To determine the correction factor, solutions with known H^+ concentrations at different ionic strengths (0.5 to 4 mol·L^{-1}) were prepared at 22 °C using $HClO_4$ and $NaClO_4$. Their pH_{exp} were measured with combination pH electrodes (SenTix® MIC from VWR). In order to avoid precipitation of $KClO_4$ in the diaphragm of the electrode, the original junction electrolyte (3 mol·L^{-1} KCl) was replaced by a 3 mol·L^{-1} NaCl solution. The electrodes were calibrated using standard buffer solutions (WTW). All pH measurements and the obtained correction factor are summarized in the Supporting Information (Figure S1 and Tables S1-S2).

Compositions of the solutions

As a first step, the impact of the ionic strength on the complexation of Eu(III) and Cm(III) with phosphate was investigated at 25 °C. The proton concentration was kept constant at 0.1 $mol \cdot L^{-1}$ and the ionic strength, imposed by $NaClO_4$, was ranging from 0.6 to 3.1 $mol \cdot L^{-1}$. According to the correction factor for pH measurements at high $NaClO_4$ concentration (SI), the pH_{exp} of the solutions at 0.6, 1.1, 2.1 and 3.1 $mol \cdot L^{-1}$ ionic strength were 0.81, 0.74, 0.56 and 0.34, respectively.

The total phosphate concentration denoted as [$\Sigma(PO_4)$], was ranging from zero to a maximum of 10 % of the total ionic strength in solution. The concentration of Eu(III) and Cm(III) were $5 \cdot 10^{-6}$ and $3 \cdot 10^{-7} - 5 \cdot 10^{-7}$ $mol \cdot L^{-1}$, respectively. In a second set of experiments the impact of elevated temperature was investigated. The solutions prepared at I = 1.1 $mol \cdot L^{-1}$ were taken and stepwise heated up to 80 °C using a HLC ThermoMixer (MKR 23 BlockThermostate, Ditabis).

Laser-induced luminescence spectroscopy

The *in situ* solution speciation of Eu(III) and Cm(III) in the presence of dissolved phosphates was investigated with laser-induced luminescence spectroscopy. The luminescence emission signal of Eu(III) and Cm(III) is sensitive to changes occurring in the metal cation coordination spheres as a result of, e.g., complexation reactions. For Cm(III) such complexation reactions will induce a shift of the emission peak position of the free aquo ion at 593.8 nm, typically to longer wavelengths (called a red-shift or bathochromic shift). In case of Eu(III), changes are seen especially in the intensity of the hypersensitive emission transition, $^5D_0 \rightarrow {}^7F_2$. These spectral changes can be used to monitor the Cm(III) and Eu(III) complexation with aqueous phosphates, and to derive species distributions that can further be used for the calculation of conditional complexation constants.

For the luminescence measurements, 3 mL of the sample volume was pipetted into quartz cuvettes. The sample temperature was kept constant at the desired temperature in a heatable cuvette holder (Quantum Northwest TL 125) during the complete duration of the measurement. The laser spectroscopic measurements were performed with a pulsed Nd:YAG (Continuum Surelite II) pump laser coupled to a solid-state optical parametric oscillator (OPO, PANTHER EX OPO, Continuum). The luminescence emission spectra

were recorded at 580 – 620 nm, 1 µs after the exciting laser pulse (λ_{ex} = 396.6 nm for Cm(III), λ_{ex} = 394 nm for Eu(III)). The luminescence emission signal was detected by an optical multichannel analyzer with a 1200 lines/mm grating and an ICCD-Camera (iStar, Andor).

Speciation calculations

To predict the concentration of free H_3PO_4, speciation was calculated with PHREEQC.[18] The ThermoChimie database (version 9b0) from ANDRA[19] using the SIT approach to deal with the activity coefficients was used. In a first step, calculations were performed at different ionic strength (0.6, 1.1. 2.1 and 3.1 mol·L^{-1} $NaClO_4$), at 25 °C and at [H^+] = 0.1 mol·L^{-1}. The total phosphate concentration, identical to those taken for the batch experiments, was ranging from $1 \cdot 10^{-4}$ to 0.15 mol·L^{-1}. Afterwards, similar calculations were performed at [H^+] = 0.1 mol·L^{-1}, but at elevated temperatures (40, 50, 60 and 80 °C).

RESULTS

Influence of the ionic strength on the complexation of Eu(III)/Cm(III) by phosphate at 25 °C

Laser spectroscopic investigations

Recorded Eu(III) and Cm(III) emission spectra for different phosphate concentrations at I = 1.1 mol·L^{-1} and T = 25 °C are presented in **Figure 1** (top). The spectra are normalized to the same $^7F_1$-band intensity in case of Eu(III) and to the total surface area in case of Cm(III). For Eu(III) the intensity of the $^7F_2$ band can be seen to increase with increasing phosphate concentration, while an additional red-shifted peak appears in the Cm(III) emission spectra. These changes can be attributed to complexation reactions occurring between the trivalent metal cations and phosphates in solution.

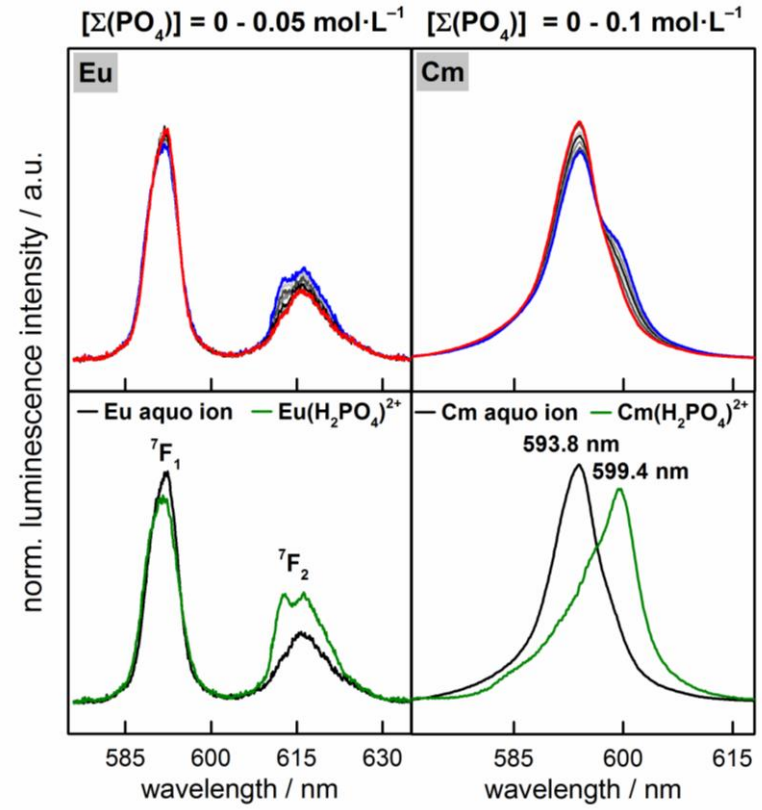

Figure 1. Normalized emission spectra of Eu(III) (top, left) and Cm(III) (top, right) recorded for various phosphate concentrations at 25 °C. (Note: The y-axis scales are different due to the different normalization procedures for Eu(III) and Cm(III) luminescence data.) Single component spectra corresponding to the free aquo ion (Me^{3+}) and the $Me(H_2PO_4)^{2+}$ (Me = Eu or Cm) complex (bottom).

To obtain pure component spectra of the individual species as well as their relative distributions and fluorescence intensity (FI) factors, the measured multicomponent spectra were deconvoluted. A comprehensive discussion of the deconvolution process can be found in Huittinen et al. 2012.[20] Two pure components were extracted from the recorded Eu(III) and Cm(III) spectra (**Figure 1**, bottom). One of the species corresponds to the free non-complexed metal aquo ion, the other one was tentatively assigned to a Eu/Cm-phosphate complex, i.e. $Eu(H_2PO_4)^{2+}$ and $Cm(H_2PO_4)^{2+}$. A detailed discussion of the assignment of this phosphate stoichiometry will be given later in the text.

The relative distributions of the involved species were obtained with least-squares fitting of the collected luminescence data using the derived pure component spectra. The distribution was thereafter corrected with the FI factors of the two species, which were determined from the measured integrated fluorescence intensity of the sum spectra with respect to the intensity of the aquo ion. By setting the relative intensity of the trivalent metal aquo ions to one (1), FI factors of 1.15 and 0.68 were found for the Eu-phosphate and Cm-phosphate species, respectively. The obtained species distributions are presented in Figure 2 (left).

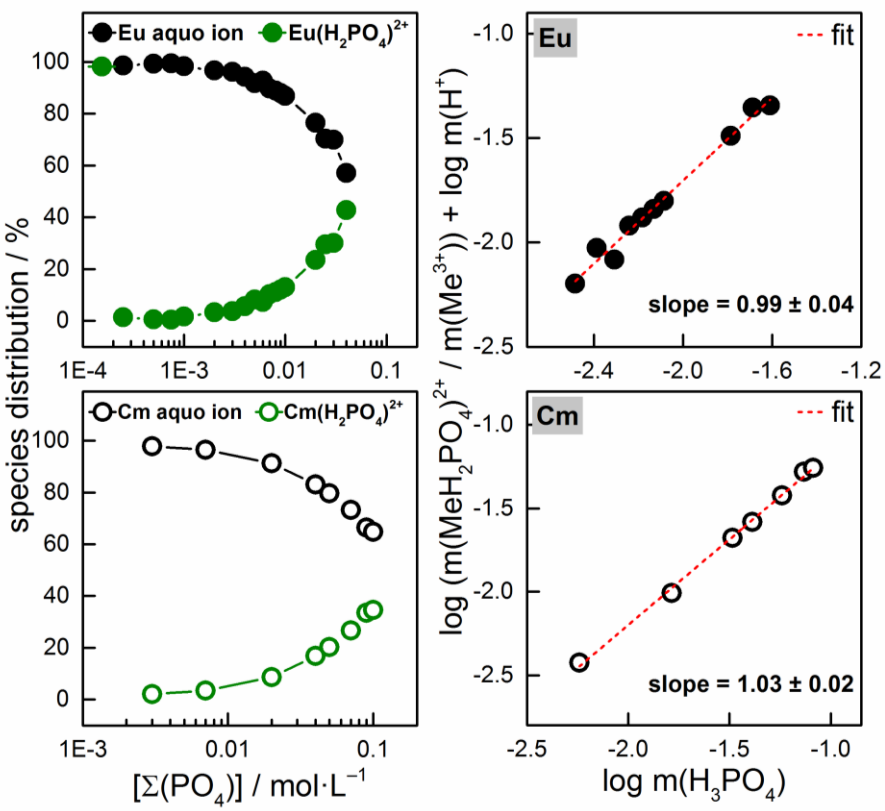

Figure 2. Left: spectroscopically derived aqueous speciation as a function of total phosphate concentration for Eu(III) (top) and Cm(III) (bottom) for I = 1.1 mol·L^{-1} and T = 25 °C. Right: slope analysis performed for the equilibrium $Me^{3+} + H_3PO_4 \rightleftharpoons MeH_2PO_4^{2+} + H^+$ (Me = Eu or Cm).

From the species distributions it is evident, that the fraction of the Eu(III)-phosphate complex exceeds that of the Cm(III)-phosphate one for similar phosphate concentrations. Thus, a larger complexation constant can be expected for the former one. With increasing ionic strength, the complexation equilibrium is shifted to the product side, i.e. the formation of Eu/Cm$(H_2PO_4)^{2+}$ is promoted at higher ionic strength. For the spectroscopic data at I = 0.6, 2.1, and 3.1 mol·L^{-1}, the reader is referred to the SI (Figures S2 and S3).

Determination of the conditional constants at 25 °C

The molar concentrations of the Eu^{3+}/Cm^{3+} aquo ions and the postulated $MeH_2PO_4^{2+}$ complexes at 25 °C and four ionic strengths were obtained from the derived species distribution (Figure 2, left and Figure S3 in SI) and converted to the molal scale. For such conversions, the required density of the $NaClO_4$ background electrolyte solutions at the given temperature and concentration was taken from Söhnel and Novotný.[21]

These molalities were thereafter used to calculate the conditional complexation constants log β(I) assuming the following equilibrium:

$Me^{3+} + H_3PO_4 \rightleftharpoons MeH_2PO_4^{2+} + H^+$ (Me = Eu or Cm)

The concentration of free phosphoric acid at the different ionic strengths under investigation was calculated in the molal scale using PHREEQC and the SIT database. At this stage, two important issues have to be discussed.

The first one is related to the values of the $\varepsilon(Na^+;H_2PO_4^-)$, $\varepsilon(Na^+;HPO_4^{2-})$, and $\varepsilon(Na^+;PO_4^{3-})$ ion interaction coefficients. Lemire et al.[22] mentioned that their recommended values (Table 1) were taken from the original values reported by Ciavatta.[23] However, after a careful examination, the ε values under discussion (Table 1) are different in both sources.[22, 23] This is due to the fact that Ciavatta[23] used a linear function $\varepsilon(j;k) = \varepsilon(1) + C \cdot \log(I)$ to calculate these ε coefficients. Lemire et al.[22] also provided ε values taking into account their ionic strength dependency and they seem to be in agreement with those reported by Ciavatta[23] (except for the C value for $\varepsilon(Na^+;HPO_4^{2-})$).

Using a recent study performed by El Guendouzi and Benbiyi[24] who determined the mean activity coefficients of NaH_2PO_4 and Na_2HPO_4 at 25°C, authors derived other values for $\varepsilon(Na^+;H_2PO_4^-)$ and $\varepsilon(Na^+;HPO_4^{2-})$, without considering an ionic strength dependency (Table 1). Due to the fact that the ionic strength dependent function is not yet implemented in any geochemical codes, any practical application has to use the interaction coefficients obtained from the linear fitting. One just needs to bear in mind these limitations.

The impact of using the values derived from El Guendouzi and Benbiyi[24] instead of those reported in Lemire et al.[22] on the final log β values was marginal ($\Delta\log\beta = 0.0025$). Thus, the $\varepsilon(Na^+;H_2PO_4^-)$, $\varepsilon(Na^+;HPO_4^{2-})$ and $\varepsilon(Na^+;PO_4^{3-})$ values recommended by Lemire et al.[22] were used in the present study for all further computations.

Table 1. Comparison of ε(Na^+;$H_2PO_4^-$), ε(Na^+;HPO_4^{2-}), and ε(Na^+;PO_4^{3-}) reported in the literature and calculated in this study

ε (kg·mol^{-1})	Lemire et al.[22]	Ciavatta[23]	This study (based on El Guendouzi and Benbiyi[24])
(Na^+;$H_2PO_4^-$)	−0.08±0.04	ε(1) = −0.11; C = 0.09[a]	−0.05±0.01
(Na^+;HPO_4^{2-})	−0.15±0.06	ε(1) = −0.19; C =0.06[a]	−0.19±0.01
(Na^+;PO_4^{3-})	−0.25±0.03	ε(1) = −0.29; C = 0.10[a]	−0.26±0.01

[a] data fitted with a linear function ε(j;k) = ε(1) + C·log(I)

The second point relates to the classical conflict between the ion interaction model and the ion association model. In the latter, the formation of ion-pairs is considered and the activity coefficients only depend on the ionic strength of the solution. Lemire et al.[22] clearly indicated that the ion interaction coefficients tabulated by Ciavatta[23] were calculated without taking into account ion pair formation. Although the Thermochimie database is based on the SIT model, it also contains formation constants of the $NaH_2PO_4^0$, $Na(HPO_4)^-$ and $NaPO_4^{2-}$ ion pairs. Neglecting the formation of these ion pairs during the calculation of the concentration of the free phosphoric acid led to an offset $\Delta\log\beta = 0.03$ in the complexation constant. Resolving such conflicts requires much more efforts and is not the scope of the present paper. Hence, a pragmatic approach was adopted: the formation of the $NaH_2PO_4^0$, $Na(HPO_4)^-$ and $NaPO_4^{2-}$ ion pairs was included and the uncertainty on each log β was increased by an absolute value of 0.03.

Since the concentrations of Eu(III) and Cm(III) were orders of magnitude lower than that of H_3PO_4, it is safe to assume that the speciation of the latter was not significantly impacted by the trivalent cations during the complexation. By applying the law of mass action, the following expression of the conditional stability constant was obtained:

$$log\beta(I) = \frac{m_{MeH_2PO_4^{2+}} m_{H^+}}{m_{Me^{3+}} m_{H_3PO_4}} \quad (2)$$

Based on Equation 2, the term $\log \frac{m_{MeH_2PO_4^{2+}}}{m_{Me^{3+}}} + \log m_{H^+}$ was plotted as a function of $\log m_{H_3PO_4}$ at an ionic strength of 1.1 mol·L^{-1} (Figure 2, right). The results of the slope analysis for the data at I = 0.6, 2.1, and 3.1 mol·L^{-1} are given in the SI (Figures S4 for Eu and Figure S5 for Cm). The slopes were systematically close to one, confirming the postulated formation of the $MeH_2PO_4^{2+}$ complex. The conditional log β, corresponding to the intercept at origin in each of the slope analysis-plots, are summarized in Table 2, together with their uncertainties.

Table 2. Thermodynamic conditional stability constants for the formation of $EuH_2PO_4^{2+}$ and $CmH_2PO_4^{2+}$ at 25 °C at varying ionic strengths

Ionic strength (mol·L^{-1})	$Eu^{3+} + H_3PO_4 \rightleftharpoons EuH_2PO_4^{2+} + H^+$	$Cm^{3+} + H_3PO_4 \rightleftharpoons CmH_2PO_4^{2+} + H^+$
0.6	0.17±0.14	−0.25±0.22
1.1	0.29±0.11	−0.14±0.10
2.1	0.34±0.18	−0.06±0.11
3.1	0.39±0.20	-

Raising the ionic strength led to an increase of the complexation constants for both $EuH_2PO_4^{2+}$ and $CmH_2PO_4^{2+}$ at 25 °C, as already suggested by the luminescence data.

Extrapolation to zero ionic strength at 25 °C

The extrapolation to infinite dilution requires the consideration of the activity coefficients. Applying SIT,[22] the activity coefficient of the species j (taking part in the reaction) interacting with species k can be expressed as:

$$log_{10}\gamma_j = -z_j^2 D + \sum_k \varepsilon(j;k) m_k \quad (3)$$

with z_j representing the charge of species j, $\varepsilon(j;k)$ being the ion interaction coefficient between species j and species k, m_k the molality of species k, and D the Debye-Hückel term:

$$D = \frac{A\sqrt{I_m}}{1+Ba_i\sqrt{I_m}} \quad (4)$$

In the Debye-Hückel term D, the term A is the Debye-Hückel constant. The NEA TDB provides a table (see Appendix B.1.2 in Lemire et al.[22]) for the temperature dependence of A, where A = 0.509 $kg^{1/2}\cdot mol^{-1/2}$ at 25 °C. The constant Ba_i was chosen as 1.5 $kg^{1/2}\cdot mol^{-1/2}$ for all temperatures up to 80 °C, as recommended by Lemire et al.[22]

The equilibrium constants at zero ionic strength and the conditional stability constants are related as follows:

$$\log_{10}\beta - \Delta z^2 D = \log_{10}\beta^\circ - \Delta\varepsilon I_m \quad (5)$$

The equilibrium $Me^{3+} + H_3PO_4 \rightleftharpoons MeH_2PO_4^{2+} + H^+$ gives:

$$\Delta\varepsilon = \varepsilon(MeH_2PO_4^{2+};ClO_4^-) + \varepsilon(H^+;ClO_4^-) - \varepsilon(Me^{3+};ClO_4^-) \quad (6)$$

The interaction coefficient $\varepsilon(H^+;ClO_4^-)$ was taken from Lemire et al.,[22] while $\varepsilon(Me^{3+};ClO_4^-)$ was estimated to be equal to $\varepsilon(Am^{3+};ClO_4^-)$ = 0.49±0.03 $kg\cdot mol^{-1}$.[22] Following the SIT formalism, the ion interaction coefficient of the uncharged species H_3PO_4 was set to zero[22]. $\Delta z^2 = \Sigma z^2$ (products) − Σz^2 (reactants) was equal to −4.

By plotting $\log_{10}\beta - \Delta z^2 D$ as a function of the ionic strength, a weighted linear regression provided logβ° (intercept with the y-axis) and −Δε (slope) (Figure 3). Detailed explanations on the performance of the weighted linear regression are provided in the SI.

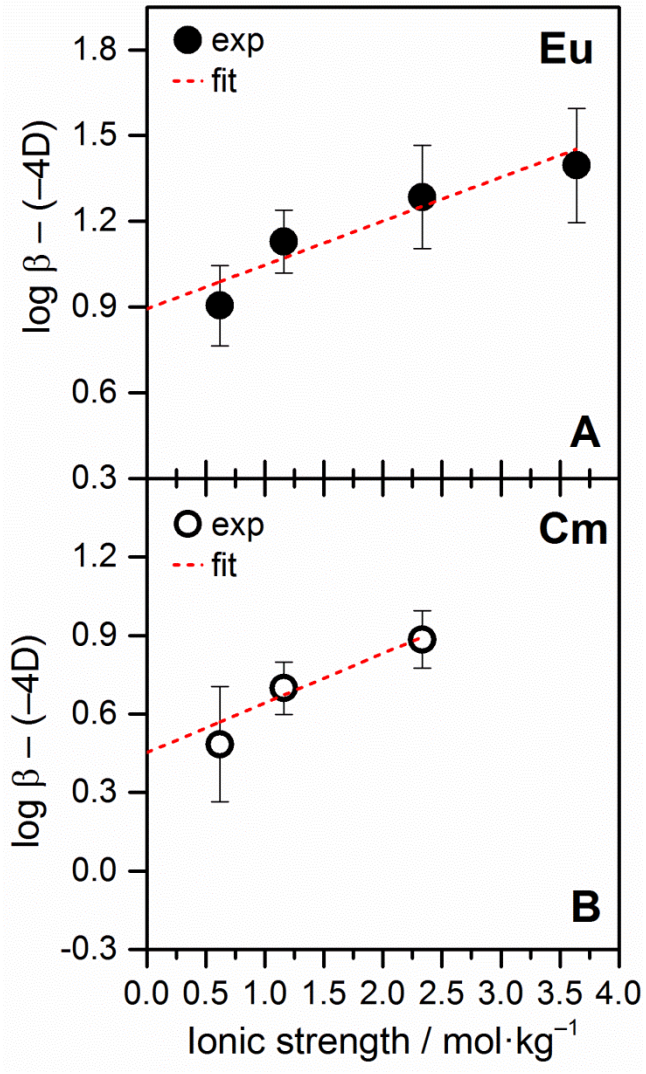

Figure 3. Linear SIT regression plot for the $MeH_2PO_4^{2+}$ complexes at 25 °C.

From the slope found to be 0.15 for Eu(III) and 0.19 for Cm(III), the $\varepsilon(MeH_2PO_4^{2+};ClO_4^-)$ were derived according to equation (6). The obtained logβ° and $\varepsilon(MeH_2PO_4^{2+};ClO_4^-)$ values are summarized in Table 3.

The uncertainties on the $\varepsilon(MeH_2PO_4^{2+};ClO_4^-)$ were calculated based on the recommendations in Appendix C in the most recent NEA volume.[22]

$$\sigma_{\varepsilon(MeH_2PO_4^{2+};ClO_4^-)} = \sqrt{(\sigma_{\Delta\varepsilon})^2 + \sigma(\varepsilon(H^+;ClO_4^-))^2 + \sigma(\varepsilon(Me^{3+};ClO_4^-))^2} \qquad (7)$$

Table 3. Complex formation constants at infinite dilution for $MeH_2PO_4^{2+}$ and ion interaction coefficients $\varepsilon(MeH_2PO_4^{2+};ClO_4^-)$ (Me = Eu or Cm) at 25 °C

Reaction	$\log_{10}\beta^\circ$	$\varepsilon(MeH_2PO_4^{2+};ClO_4^-)$ (kg·mol^{-1})
$Eu^{3+} + H_3PO_4 \rightleftharpoons EuH_2PO_4^{2+} + H^+$	0.89±0.13	0.20±0.08
$Cm^{3+} + H_3PO_4 \rightleftharpoons CmH_2PO_4^{2+} + H^+$	0.45±0.19	0.16±0.12

Influence of temperature on the complexation of Eu^{3+}/Cm^{3+} by phosphate

Laser-induced luminescence spectroscopy

Luminescence data were collected for Eu(III) and Cm(III) at 25, 40, 50, 60, and 80 °C. The evolution of the emission spectra in the presence of $[\Sigma(PO_4)]$ = 0.02 mol·L^{-1} as a function of temperature is shown in **Error! Reference source not found.** (left) for Eu(III) (top) and Cm(III) (bottom) (a larger selection of emission spectra at 40 °C and 60 °C is presented in the SI, Figure S6).

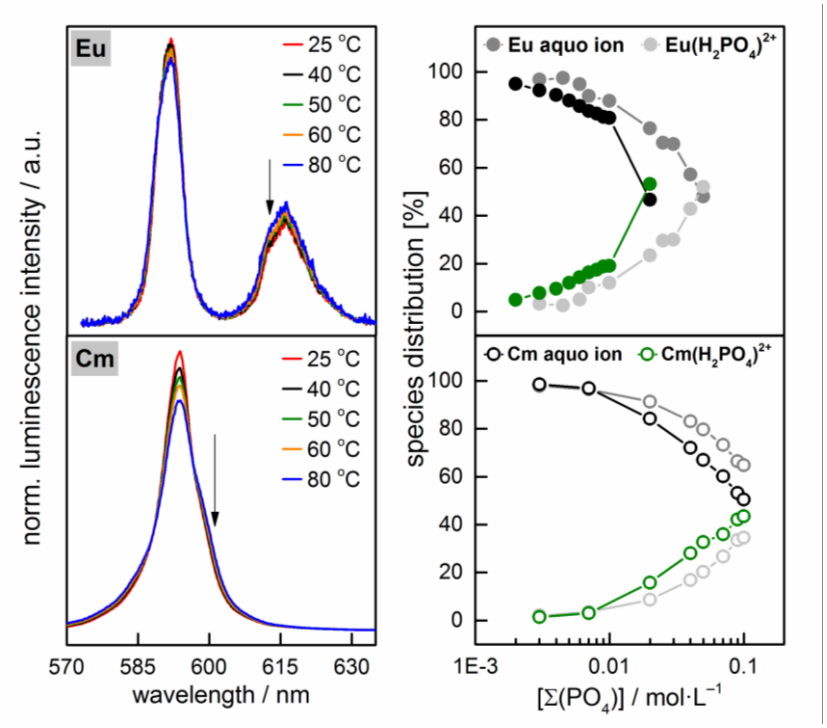

Figure 4. Left: measured Eu(III) (top) and Cm(III) (bottom) emission spectra in the presence of 0.02 mol·L^{-1} phosphate ($[\Sigma(PO_4)]$) at varying temperatures. Right: derived species distributions at 25 °C (gray symbols) and 80 °C (black and green symbols) for Eu(III) (top) and Cm(III) (bottom).

The temperature-induced differences in the emission spectra are small. For Eu(III), the intensity of the $^7F_1$-band slightly decreases, while the opposite is true for the hypersensitive $^7F_2$-band (denoted in Figure 4 (top, left) with an arrow). In case of Cm(III), the intensity of the peak corresponding to the aquo ion decreases, while a slight shoulder on the right side appears (indicated with an arrow in **Error! Reference source not found.**, bottom, left). These changes can be attributed to a subtle increase of the Eu(III)/Cm(III)-phosphate complexation with increasing temperature. This increase is further confirmed when comparing the derived species distribution at 80 °C (black and green symbols) with the distribution obtained at 25 °C (gray symbols) (Figure 4, right). Here, it is clearly visible that the amount of $Me(H_2PO_4)^{2+}$ for a given phosphate concentration is larger at 80 °C than at 25 °C. Similar species distributions were derived for all investigated temperatures using the FI factors obtained at 25 °C, allowing for the determination of conditional complexation constants as described below.

Determination of the conditional constants at elevated temperature

According to the pH_{exp} measurements at elevated temperatures and at an ionic strength of 1.1 mol·L^{-1}, the difference compared to the pH_{exp} of samples at 25 °C was not exceeding 0.05, which is within the uncertainty range of the pH measurement. Consequently, the molality of H^+ was assumed to be identical to the one at 25 °C during all speciation calculations.

Following the same methodology described above, the term $\log \frac{m_{MeH_2PO_4^{2+}}}{m_{Me^{3+}}} + \log m_{H^+}$ was plotted as a function of $\log m_{H_3PO_4}$ at an ionic strength of 1.1 mol·L^{-1} and at 40, 50, 60 and 80 °C (see Figure S7 for Eu(III) and Figure S8 for Cm(III) in SI). All slopes were close to one, indicating no change in the stoichiometry of the formed complexes, i.e. $EuH_2PO_4^{2+}$ and $CmH_2PO_4^{2+}$, upon increasing temperature. All resulting conditional log β values for $EuH_2PO_4^{2+}$ and $CmH_2PO_4^{2+}$ are summarized in Table 4, together with their uncertainties. The uncertainties on log β°(T) were obtained from the uncertainties on log β(T) and Δε as follows:

$$\sigma_{log\beta^0} = \sqrt{\sigma^2_{\log\beta} + (m_{ClO_4^-}\sigma_{\Delta\varepsilon})^2} \quad (8)$$

Table 4. Thermodynamic conditional (I = 1.1 mol·L^{-1}) and extrapolated to infinite dilution stability constants for the formation of $EuH_2PO_4^{2+}$ and $CmH_2PO_4^{2+}$ at 25, 40, 50, 60 and 80 °C

	$Eu^{3+} + H_3PO_4 \rightleftharpoons EuH_2PO_4^{2+} + H^+$		$Cm^{3+} + H_3PO_4 \rightleftharpoons CmH_2PO_4^{2+} + H^+$	
Temperature (°C)	log β	log β°	log β	log β°
25	0.29±0.11	0.89±0.13	−0.14±0.10	0.45±0.19
40	0.35±0.15	1.04±0.17	−0.12±0.10	0.52±0.16
50	0.39±0.15	1.10±0.17	−0.08±0.20	0.58±0.24
60	0.45±0.18	1.18±0.20	−0.02±0.10	0.66±0.16
80	0.52±0.13	1.29±0.15	0.02±0.10	0.74±0.16

Upon increasing the temperature, the equilibrium $Me^{3+} + H_3PO_4 \rightleftharpoons MeH_2PO_4^{2+} + H^+$ was shifted towards the product side, indicating a favored complexation reaction.

Extrapolation to zero ionic strength

The SIT approach[22] was used for the extrapolation to zero ionic strength, according to equation 5. The Debye-Hückel constant A in the Debye-Hückel term was taken from the tabulated values by Lemire et al.[22] at 40 °C (0.523 $kg^{1/2}\cdot mol^{-1/2}$) and 50 °C (0.534 $kg^{1/2}\cdot mol^{-1/2}$). Respective values at 60 °C (0.546 $kg^{1/2}\cdot mol^{-1/2}$) and 80 °C (0.571 $kg^{1/2}\cdot mol^{-1/2}$) were calculated according to the methodology described by Moog and Voigt.[25]

According to Lemire et al.[22], the temperature dependency of the interaction coefficients ε can be neglected in the temperature range from 25 to 200 °C (with $(\partial\varepsilon/\partial T)_p < 0.005$ kg·mol^{-1}·K^{-1} at T < 200 °C). Thus, they were assumed constant in this work. Since the same equilibrium was considered, i.e. $Me^{3+} + H_3PO_4 \rightleftharpoons MeH_2PO_4^{2+} + H^+$, Δz^2 remains constant at −4. The obtained log β° values at 40, 50, 60 and 80 °C for $EuH_2PO_4^{2+}$ and $CmH_2PO_4^{2+}$ are summarized in Table 4.

Derivation of thermodynamic parameters

The molal standard enthalpy of reaction $\Delta_R H_m^0$ as well as the molal standard entropy of reaction $\Delta_R S_m^0$ were derived from an Arrhenius plot ($logK^0(T)$ as a function of the reciprocal temperature) using the integrated van't Hoff equation, *cf.* Figure 5:

$$logK^0(T) = logK^0(T_0) + \frac{\Delta_R H_m^0(T_0)}{Rln(10)}\left(\frac{1}{T_0} - \frac{1}{T}\right) \quad (9)$$

R being the universal molar gas constant (8.314 $J \cdot K^{-1} \cdot mol^{-1}$) and T the temperature in Kelvin (T_0 = 298.15 K).

In the temperature range from 25 to 80 °C, the molal heat capacity of reaction $\Delta_R C_{p,m}^0$ was assumed to be zero and the change in enthalpy $\Delta_R H_m^0$ constant. Such an approximation was already shown to be valid until 100 °C for complexation studies of actinides and lanthanides with organic and inorganic ligands.[26-28]

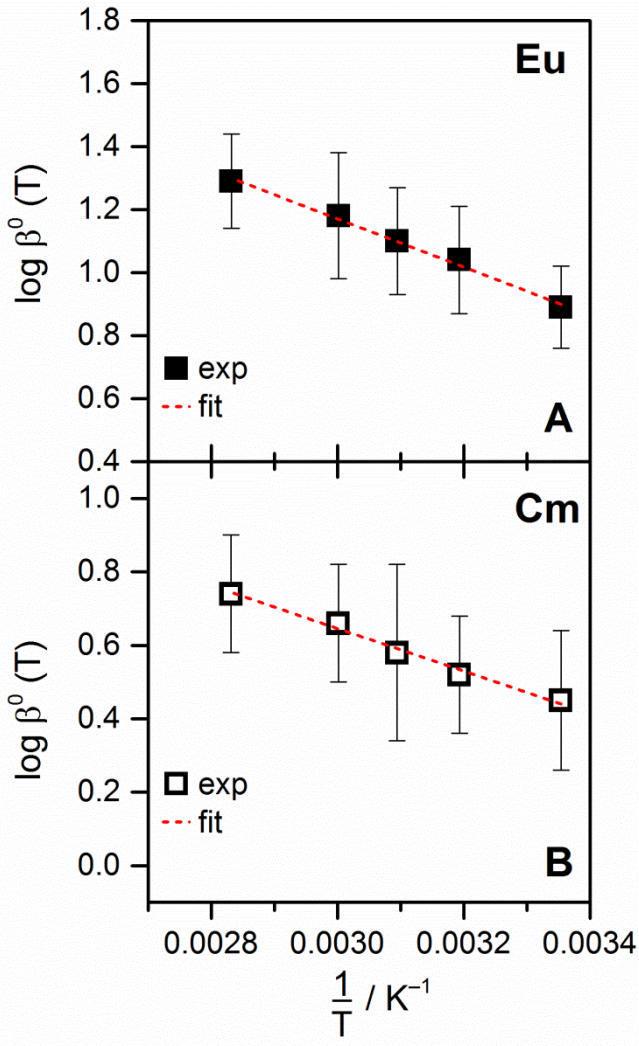

Figure 5. Arrhenius plots for Eu(III) and Cm(III) based on the data in Table 4.

The derived $\Delta_R H_m^0$ were 14.7 and 11.1 kJ·mol^{-1} for Eu(III) and Cm(III), respectively, whereas $\Delta_R S_m^0$ were 66.4 and 45.8 J·mol^{-1} for Eu(III) and Cm(III), respectively. In other words, positive enthalpies and entropies of reaction were obtained for both Eu(III) and Cm(III) complexation reactions.

DISCUSSION

The complexation of Eu(III) and Cm(III) with phosphate ions was, as a first step, investigated at 25 °C, at four ionic strengths (0.6 to 3.1 mol·L^{-1}). The complexation constants for both Eu(III) and Cm(III) were observed to increase with increasing ionic strength, see Table 2. This can be understood when examining the impact of perchlorate anions on the first and second hydration shells of the Eu^{3+} and Cm^{3+} aquo ions. H_2O molecules in the second hydration shell are associated to the 1st hydration shell via H-bonding. There is a constant exchange of the H_2O molecules between the 1st and the 2nd hydration shell as well as with the bulk water. In combined laser-induced luminescence spectroscopic and computational (density functional theory and molecular dynamics simulations) investigations of the Cm(III)-$HClO_4$ system in concentrated perchlorate (0.3 to 9 mol·L^{-1}) solutions, the penetration of perchlorate ions into the second hydration shell of Cm(III) was suggested, as well as the ability of ClO_4^- ions to form weak H-bonds with the H_2O molecules in the 1st hydration shell (Trumm and Lindqvist-Reis[29]). Formation of solvent-shared ion pairs was also evidenced, leading to a weakening of the binding of H_2O molecules in the first hydration shell of the Cm^{3+} aquo ion. This weakening can be expected to increase upon raising the concentration of perchlorate ions, enabling the $H_2PO_4^-$ ion to exchange one water molecule from the 1st hydration shell more easily. In addition, increasing the ionic strength leading to a decreasing water activity leads to a reduced number of water molecules available for the 2nd hydration shell, due to the hydration of the ions of the background electrolyte. The above mentioned phenomena together with the increase of the short range interactions of the formed $MeH_2PO_4^{2+}$ complex with the perchlorate ions are part of the mechanisms governing the increasing log β upon increasing ionic strength.

Based on the complexation experiments at elevated temperatures, both positive enthalpies and entropies of reaction were assessed. The observed positive enthalpic term (endothermic reaction) implies that the heat required to disrupt the first hydration shell and break the Eu/Cm-H_2O bonds (endothermic) is higher than the heat released when forming bonds between Eu^{3+}/Cm^{3+} and the $H_2PO_4^-$ molecules (exothermic). This unfavorable enthalpy of reaction indicates that the heat spent in the dehydration step is not regained during the formation of the complex.

The entropic term ΔS, is a measure of the overall change in the order of the system during the complexation reaction. The reaction between the Eu^{3+}/Cm^{3+} and $H_2PO_4^-$ ions disrupt the water network around the metal ions, and leads to a release of water molecules into the network of the bulk solvent. Since there is a release of constrained water molecules from the 1st hydration shell, the disorder of the system increases and consequently the entropy increases. In addition, the entropy contribution from dehydration of the aquo ions and liberation of water molecules is more significant than the loss of entropy coming from the association of the Eu^{3+}/Cm^{3+} ions with the $H_2PO_4^-$ ligand and the new structure of the water molecules around the formed $MeH_2PO_4^{2+}$ complex. The positive reaction entropy overcomes the unfavorable enthalpic component to promote the complex formation, referred to as the so called compensation effect.[30] To summarize, the energy required for the dehydration of the Me^{3+} ions contributes to the positive enthalpy change, whereas the release of water molecules from the hydration shell is responsible for the positive entropy of reaction.

The complexation was enhanced at higher temperature (see Figure 4 and Table 4), due to the increase of the entropic term. Indeed, at elevated temperature, the structure of the bulk water gets more disordered due to the higher thermal motion. The release of water molecules into a more disordered bulk water leads to a larger gain in the entropy of reaction at higher temperatures.

The complexation constant at the different ionic strengths and temperatures were found to be higher for $EuH_2PO_4^{2+}$ than for $CmH_2PO_4^{2+}$ (Table 2 and Table 4). The difference is rather remarkable, i.e. 0.44 log units at infinite dilution and T = 25 °C. Within the primary solvation shell, the bond strength between the metal ion and the water molecules increases with the electrical charge of the metal ion and decreases with its radius. Since the size of the Eu^{3+} aquo ion is slightly smaller than that of Cm^{3+}, as can be deduced from the average reported Me-O distances of the tricapped-trigonal-prismatic aquo ions (2.470 Å[31] for Eu^{3+} vs. 2.484 Å[32] for Cm^{3+}), the charge density z/r^2 is higher for the former one. This would imply that the strength of the bond between Eu^{3+} and H_2O molecules is slightly stronger than between Cm^{3+} and H_2O molecules. Since the water molecules are more constrained around Eu^{3+} than Cm^{3+}, the increase of entropy due to the release of water molecules during the complexation with $H_2PO_4^-$ is higher for Eu(III)

than for Cm(III), which could partly explain the higher complexation constant for Eu(III) in comparison to Cm(III). Based on our spectroscopic data, further insight into possible underlying reasons for the different complexation constants obtained for the Eu(III) and Cm(III) phosphate species are difficult to give, and is beyond the scope of the present study.

The interaction coefficient $\varepsilon(Me(H_2PO_4)^{2+};ClO_4^-)$ was found to be larger for Eu (0.20±0.08 kg·mol^{-1}) than for Cm (0.16±0.12 kg·mol^{-1}). This is attributed to the higher charge density of the smaller $Eu(H_2PO_4)^{2+}$ complex as discussed above in connection to the relative Eu-H_2O vs. Cm-H_2O bond strengths of the metal aquo ions. Note that Lemire et al.[22] recommended an even larger value of 0.39±0.04 kg·mol^{-1} for $\varepsilon(AmH_2PO_4^{2+};ClO_4^-)$, estimated by Silva et al.[7] from the $\varepsilon(YHCO_3^{2+};ClO_4^-)$ ion interaction coefficient. That estimation was purely based on charge consideration, ignoring the vast differences in the complex structure of $AmH_2PO_4^{2+}$ and $YHCO_3^{2+}$. In order to provide reasonable "default values" when data were lacking, Thoenen et al.[33] performed a thorough statistical analysis of all published SIT interaction coefficients in $NaClO_4$ media, based on charge considerations only. The following relation was found: $\varepsilon(M^{n+};ClO_4^-)$ = charge × 0.2, meaning that $\varepsilon(Eu(H_2PO_4)^{2+};ClO_4^-)$ and $\varepsilon(Cm(H_2PO_4)^{2+};ClO_4^-)$ should have been 0.40 kg·mol^{-1}. Our values differ significantly from those recommended by Lemire et al.[22] and Thoenen et al.[33], probably because they simply neglect the size and structure of the resulting complex (e.g. its electron density distribution). Thus, such estimations should be used extremely carefully.

The parameters derived in this work were compared with those in the literature, for the equilibrium $Me^{3+} + H_3PO_4 \rightleftharpoons MeH_2PO_4^{2+} + H^+$. This data was recalculated using the reaction $H^+ + H_2PO_4^- \rightleftharpoons H_3PO_4$ ($\log_{10}\beta^\circ = 2.14$) from Lemire et al[22]. The $\log_{10}\beta^\circ$ for Cm at 25 °C was found to be in good agreement with the one reported by Moll et al.[10] (Figure 6).

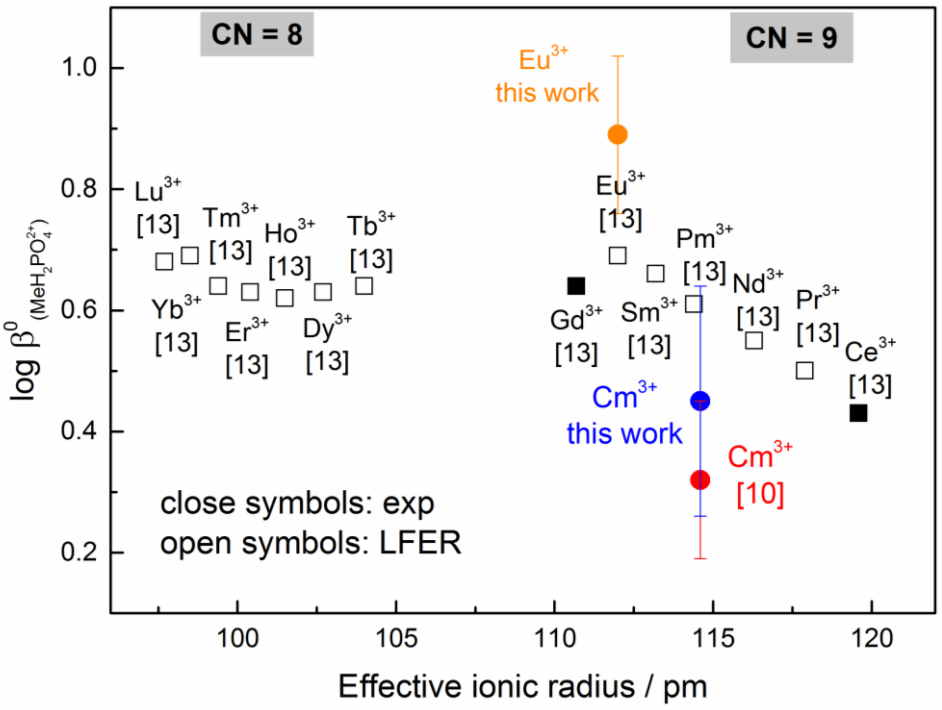

Figure 6. Comparison of log β° for $MeH_2PO_4^{2+}$ (Me = Ln, An) at 25 °C for the Me^{3+} + H_3PO_4 ⇌ $MeH_2PO_4^{2+}$ + H^+ equilibrium between this study and the literature. The effective ionic radii for the lanthanides and actinides are taken from Shannon (1976)[34] and David and Vokhmin (2003)[35] and refer to a coordination number of 8 (Lu-Tb) and 9 (Gd-Ce + Cm).

Figure 6 also shows former reported values for actinides (Cm) and lanthanides at 25 °C. It can be clearly seen that our $\log_{10}\beta^{\circ}$ for Eu is significantly higher than those reported before, which are based on linear free energy relationships from Ce and Gd data.[5] It now becomes clear that it would be worth to experimentally determine respective data for several other lanthanides, similarly to what was done for Eu in this work. This would allow for a more trustworthy application of LFER to close the remaining gaps.

The prediction of the aqueous behavior of REE under hydrometallurgical relevant chemo-technical conditions (high temperatures and high ionic strengths arising from the use of highly concentrated strong acids) has to rely on accurate thermodynamic data such as REE complexation constants towards inorganic ligands. The same applies for actinides in the context of nuclear waste disposal, where the mobility of these radioactive contaminants has to be accounted for in a variety of environmental conditions.

The new thermodynamic data derived in this fundamental study will support the optimization of technological strategies applied to access raw materials and contribute to a fundamental process understanding necessary to critically assess the environmental fate of REE and actinides.

ASSOCIATED CONTENT

The Supporting Information is available free of charge on the ACS Publications website at DOI:

pH measurements to obtain the correction factor in high ionic strength ($NaClO_4$). Laser-induced fluorescence spectroscopy data at 0.6, 2.1 and 3.1 $mol \cdot L^{-1}$ at 25 °C and at 1.1 $mol \cdot L^{-1}$ at 40, 50, 60 and 80 °C, with their respective species distribution and slope analysis.

AUTHOR INFORMATION

Corresponding Authors

*E-mail: n.jordan@hzdr.de

*E-mail: n.huittinen@hzdr.de

ORCID

Norbert Jordan: 0000-0002-4625-1580

Vinzenz Brendler: 0000-0001-5570-4177

Nina Huittinen: 0000-0002-9930-2329

Notes

The authors declare no competing financial interest.

ACKNOWLEDGMENTS

The authors would like to thank the German Federal Ministry of Education and Research (BMBF) for funding the SEM^2 (033R127D) and ThermAc (02NUK039B) projects. Xavier Gaona from KIT-INE and the technical team of the Surface processes division at HZDR- Institute of Resource Ecology are acknowledged for their help and advice regarding the pH and inductively coupled plasma-mass spectrometry measurements.

References

1.Kumari, A.; Panda, R.; Jha, M. K.; Kumar, J. R.; Lee, J. Y., *Minerals Engineering* **2015,** *79*, 102-115.
2.Ewing, R. C.; Wang, L., *Reviews in Mineralogy and Geochemistry* **2002,** *48*, 673-699.
3.Neumeier, S.; Arinicheva, Y.; Ji, Y.; Heuser, J. M.; Kowalski, P. M.; Kegler, P.; Schlenz, H.; Bosbach, D.; Deissmann, G., *Radiochimica Acta* **2017,** *105*.
4.Oelkers, E. H.; Montel, J.-M., *Elements* **2008,** *4*, 113-116.
5.Byrne, R. H.; Lee, J. H.; Bingler, L. S., *Geochimica Et Cosmochimica Acta* **1991,** *55*, 2729-2735.
6.Hummel, W.; Berner, U.; Curti, E.; Pearson, F. J.; Thoenen, T. *Nagra/PSI Chemical Thermodynamic Data Base 01/01*; 2002.
7.Silva, R. J.; Bidoglio, G.; Rand, M. H.; Robouch, P. B.; Wanner, H.; Puigdomenech, I., *Chemical Thermodynamics of Americium*. Elsevier: North-Holland, 1995.
8.Rao, V. K.; Mahajan, G. R.; Natarajan, P. R., *Radiochimica Acta* **1986,** *40*, 145-149.
9.Morgenstern, A. Humat-und Phosphatkomplexierung von Actinidionen im grundwasserrelevanten pH-Bereich. Technische Universität München, Garching, 1997.
10.Moll, H.; Brendler, V.; Bernhard, G., *Radiochimica Acta* **2011,** *99*, 775-782.
11.Du Fou de Kerdaniel, E.; Clavier, N.; Dacheux, N.; Terra, O.; Podor, R., *Journal of Nuclear Materials* **2007,** *362*, 451-458.
12.Gausse, C.; Szenknect, S.; Qin, D. W.; Mesbah, A.; Clavier, N.; Neumeier, S.; Bosbach, D.; Dacheux, N., *European Journal of Inorganic Chemistry* **2016,** *2016*, 4615-4630.
13.Liu, X.; Byrne, R. H., *Geochimica et Cosmochimica Acta* **1997,** *61*, 1625-1633.
14.Altmaier, M.; Metz, V.; Neck, V.; Muller, R.; Fanghänel, T., *Geochimica Et Cosmochimica Acta* **2003,** *67*, 3595-3601.
15.Altmaier, M.; Neck, V.; Fanghänel, T., *Radiochimica Acta* **2008,** *96*, 541-550.
16.Fanghänel, T.; Neck, V.; Kim, J. I., *Journal of Solution Chemistry* **1996,** *25*, 327-343.
17.Felmy, A. R.; Rai, D.; Mason, M. J., *Radiochimica Acta* **1991,** *55*, 177-185.
18.Parkhurst, D. L.; Apello, C. A. J. *User's guide to PHREEQC (version 2) – A computer program for speciation, batch-reaction, one dimensional transport, and inverse geochemcal calculations*, 1999.
19.Giffaut, E.; Grivé, M.; Blanc, P.; Vieillard, P.; Colàs, E.; Gailhanou, H.; Gaboreau, S.; Marty, N.; Madé, B.; Duro, L., *Applied Geochemistry* **2014,** *49*, 225–236.
20.Huittinen, N.; Rabung, T.; Schnurr, A.; Hakanen, M.; Lehto, J.; Geckeis, H., *Geochimica Et Cosmochimica Acta* **2012,** *99*, 100-109.
21.Söhnel, O.; Novotný, P., *Densities of aqueous solutions of inorganic substances*. Elsevier: Amsterdam, 1985.
22.Lemire, R. J.; Berner, U.; Musikas, C.; Palmer, D. A.; Taylor, P.; Tochiyama, O., *Chemical Thermodynamics of Iron: Part I.* OECD Publications: Paris, 2013.
23.Ciavatta, L., *Annali Di Chimica* **1980,** *70*, 551-567.
24.El Guendouzi, M.; Benbiyi, A., *Fluid Phase Equilibria* **2014,** *369*, 68-85.
25.Moog, H. C.; Voigt, W. *Thermodynamic Reference Database. Dielectric Constant, Vapor Pressure, and Density of Water and the Calculation of Debye-Hückel Parameters A_{DH}, B_{DH}, and A^{ϕ} for Water. THEREDA Technical Paper*; 2011.
26.Fröhlich, D. R.; Skerencak-Frech, A.; Morkos, M. L. K.; Panak, P. J., *New Journal of Chemistry* **2013,** *37*, 1520-1528.

27.Skerencak, A.; Panak, P. J.; Neck, V.; Trumm, M.; Schimmelpfennig, B.; Lindqvist-Reis, P.; Klenze, R.; Fanghänel, T., *Journal of Physical Chemistry B* **2010,** *114*, 15626-15634.
28.Skerencak-Frech, A.; Maiwald, M.; Trumm, M.; Fröhlich, D. R.; Panak, P. J., *Inorganic Chemistry* **2015,** *54*, 1860-1868.
29.Trumm, M.; Lindqvist-Reis, P. *Structure and vibrational spectra of the Cm(III)-$HClO_4$ system*; 2014; p 77.
30.Choppin, G. R.; Morgenstern, A., *Solvent Extraction and Ion Exchange* **2000,** *18*, 1029-1049.
31.D'Angelo, P.; Zitolo, A.; Migliorati, V.; Chillemi, G.; Duvail, M.; Vitorge, P.; Abadie, S.; Spezia, R., *Inorg Chem* **2011,** *50*, 4572-9.
32.Skanthakumar, S.; Antonio, M. R.; Wilson, R. E.; Soderholm, L., *Inorganic Chemistry* **2007,** *46*, 3485-3491.
33.Thoenen, T.; Hummel, W.; Berner, U.; Curti, E. *The PSI/Nagra Chemical Thermodynamic Database 12/07. PSI Bericht Nr. 14-04*; Paul Scherrer Institut, Villigen PSI, Switzerland 2014.
34.Shannon, R. D., *Acta Crystallographica Section A* **1976,** *32*, 751-767.
35.David, F. H.; Vokhmin, V., *New Journal of Chemistry* **2003,** *27*, 1627.

FOR TABLE OF CONTENTS ONLY

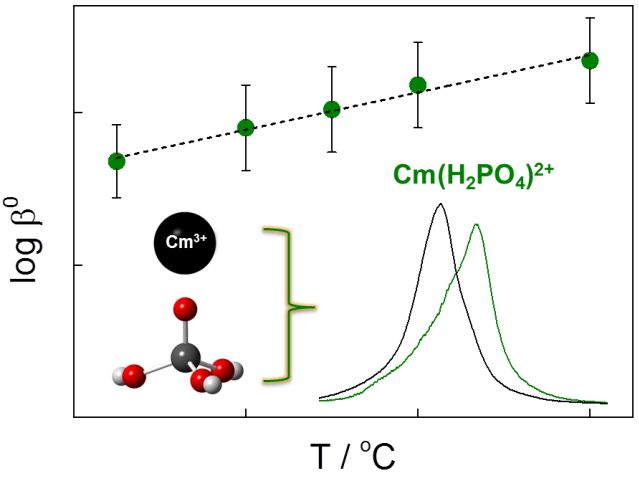

TOC Synopsis

This study investigates the complexation of Eu(III) and Cm(III) with aqueous phosphates at elevated temperature. Laser luminescence spectroscopy is used to identify the numbers of species in solution and their stoichiometry. The formation of $Eu(H_2PO_4)^{2+}$ and $Cm(H_2PO_4)^{2+}$ were identified. Their respective complexation constants increased with increasing ionic strength and temperature. The extrapolation to infinite dilution ($\log_{10}\beta^{\circ}$) was done using the specific ion interaction theory.

Complexation of trivalent lanthanides (Eu) and actinides (Cm) with aqueous phosphates at elevated temperatures

N. Jordan[1,*], M. Demnitz[1], H. Lösch[1], S. Starke[2], V. Brendler,[1] N. Huittinen[1,*]

[1]*Helmholtz-Zentrum Dresden – Rossendorf, Institute of Resource Ecology, Bautzner Landstraße 400. 01328 Dresden. Germany*

[2]*Helmholtz-Zentrum Dresden – Rossendorf, Computational Science Group (FWCC), Department of Information Services and Computing (FWC), Bautzner Landstraße 400, 01328 Dresden, Germany*

**Corresponding author:*
Phone: ++49 351 260 2148. E-mail: n.jordan@hzdr.de
Phone: ++49 351 260 2148. E-mail: n.huittinen@hzdr.de

This Supporting Information contains 13 pages, 8 figures and 2 tables.

pH measurements

To determine the correction factor, solutions at known H^+ concentrations at different ionic strength (0.5 to 4 $mol \cdot L^{-1}$) were prepared at 22 °C using $HClO_4$ and $NaClO_4$. The pH_{exp} values given in Table S1 are based on at least 3 measurements.

Table S1. H^+ concentration, ionic strength, pH_{exp} of the $HClO_4/NaClO_4$ solutions used to determine the correction factor for pH measurement at high ionic strength

$-\log [H^+]$	$[H^+]$ (mol·L^{-1})	I (mol·L^{-1})	pH_{exp}	A_c	A_c (mean)
1.700	0.0200	0.50	1.59	0.11	
2.000	0.0100	0.50	1.87	0.13	
2.125	0.0075	0.50	2.00	0.13	0.12
2.300	0.0050	0.50	2.19	0.11	
2.600	0.0025	0.50	2.47	0.13	
1.700	0.0200	0.75	1.48	0.23	
2.000	0.0100	0.75	1.78	0.22	
2.125	0.0075	0.75	1.95	0.18	0.22
2.300	0.0050	0.75	2.09	0.22	
2.600	0.0025	0.75	2.36	0.25	
1.700	0.0200	1.5	1.39	0.31	
2.000	0.0100	1.5	1.69	0.31	
2.125	0.0075	1.5	1.86	0.27	0.31
2.300	0.0050	1.5	2.01	0.29	
2.600	0.0025	1.5	2.23	0.38	
1.700	0.0200	2.0	1.28	0.42	
2.000	0.0100	2.0	1.58	0.42	
2.125	0.0075	2.0	1.72	0.40	0.42
2.300	0.0050	2.0	1.88	0.42	
2.600	0.0025	2.0	2.15	0.45	
1.700	0.0200	3.0	1.00	0.70	
2.000	0.0100	3.0	1.38	0.62	
2.125	0.0075	3.0	1.53	0.60	0.65
2.300	0.0050	3.0	1.67	0.63	
2.600	0.0025	3.0	1.92	0.68	
1.700	0.0200	4.0	0.81	0.89	
2.000	0.0100	4.0	1.15	0.85	
2.125	0.0075	4.0	1.30	0.83	0.88
2.300	0.0050	4.0	1.35	0.95	
2.600	0.0025	4.0	1.70	0.90	

For each ionic strength and for the different proton concentrations used, an average A_c factor was calculated. A polynomial fit was applied to correlate the A_c factor with the ionic strength (Figure S1).

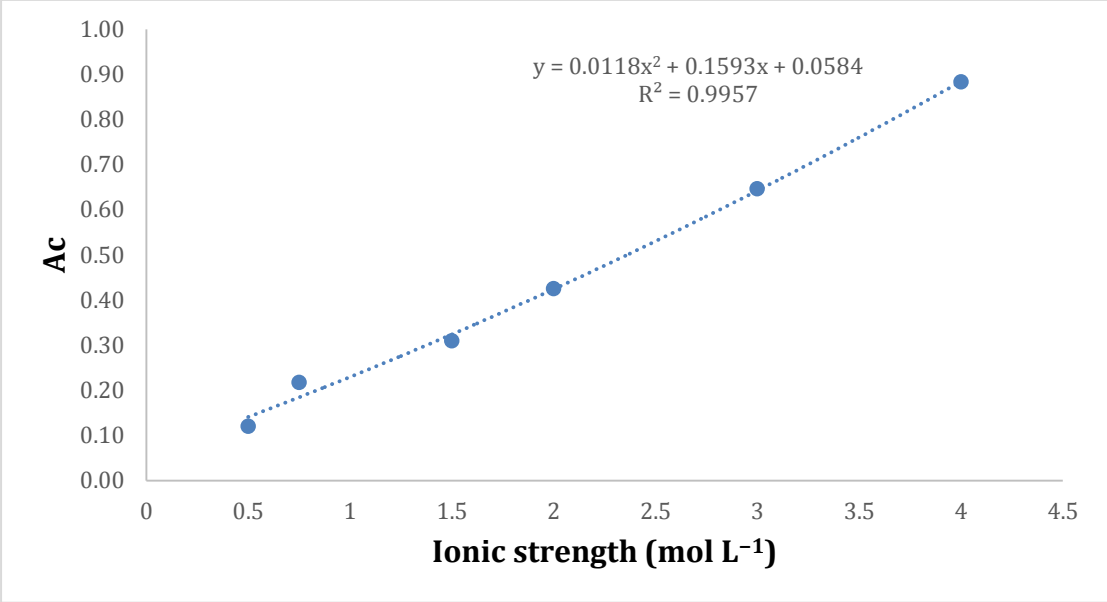

Figure S1. Correction factor A_c as a function of the ionic strength.

The following formula was derived:

$A_c = 0.0118 \times I^2 + 0.1593 \times I + 0.0584$

(I being the ionic strength in $mol \cdot L^{-1}$)

Consequently, since we worked at constant H^+ concentration (0.1 $mol \cdot L^{-1}$) and at I = 0.6, 1.1, 2.1 and 3.1 $mol \cdot L^{-1}$, the following pH_{exp} were used (Table S2).

Table S2. Correction factor and pH values for the samples prepare at high $NaClO_4$ ionic strength and constant $[H^+]$

I ($mol \cdot L^{-1}$)	$-\log [H^+]$	A_c	pH_{exp}
0.6	1.00	0.16	0.84
1.1	1.00	0.25	0.75
2.1	1.00	0.44	0.56
3.1	1.00	0.67	0.33

Laser spectroscopic investigations at T = 25 °C, I = 0.6 mol·L^{-1}, 2.1 mol·L^{-1}, and 3.1 mol·L^{-1}

The emission spectra collected at ionic strengths other than I = 1.1 mol·L^{-1} at varying total phosphate concentrations are presented in Figure S2 below.

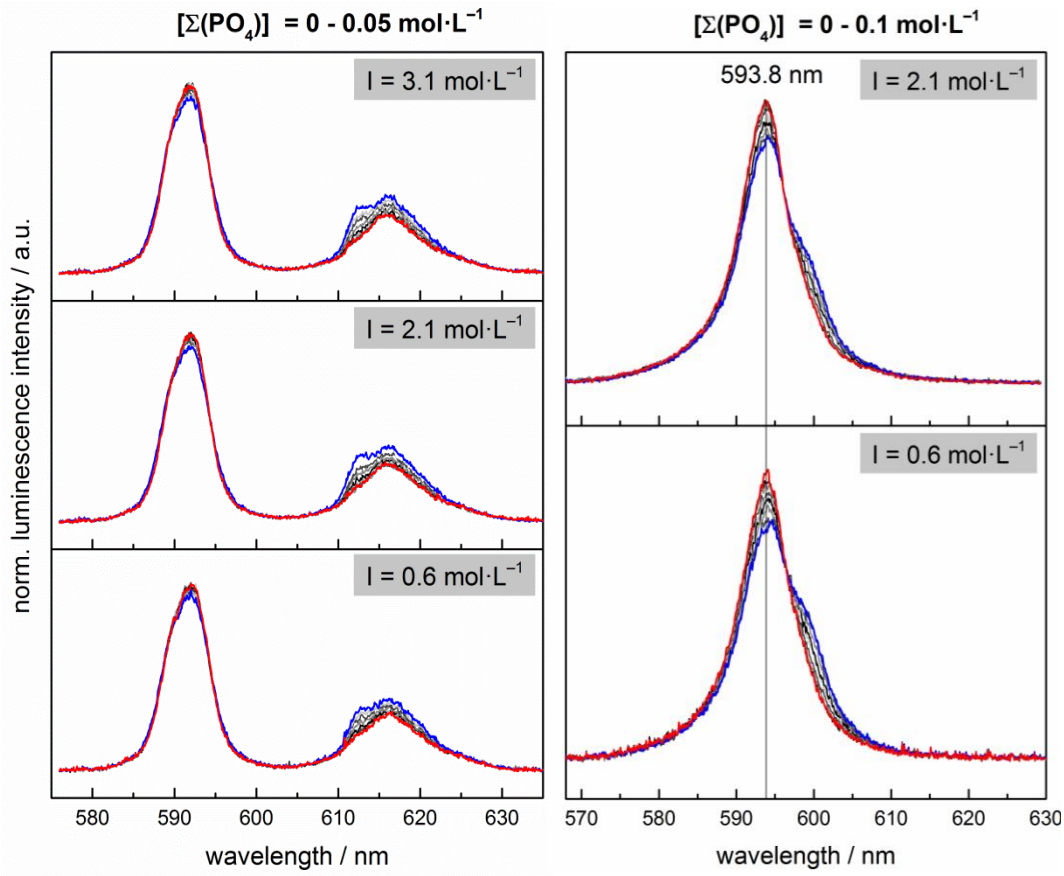

Figure S2. Recorded emission spectra at various ionic strengths and total phosphate concentrations for Eu(III) (left) and Cm(III) (right) at 25 °C.

Deconvolution of the collected sum spectra yielded the same two pure components for all investigated ionic strengths as described for I = 1.1 mol·L^{-1} in the main text, i.e. the free non-complexed metal aquo ion, and the Eu/Cm-phosphate complex Eu/Cm$(H_2PO_4)^{2+}$. From these pure component spectra, ionic strength-dependent species distributions could be derived, Figure S3.

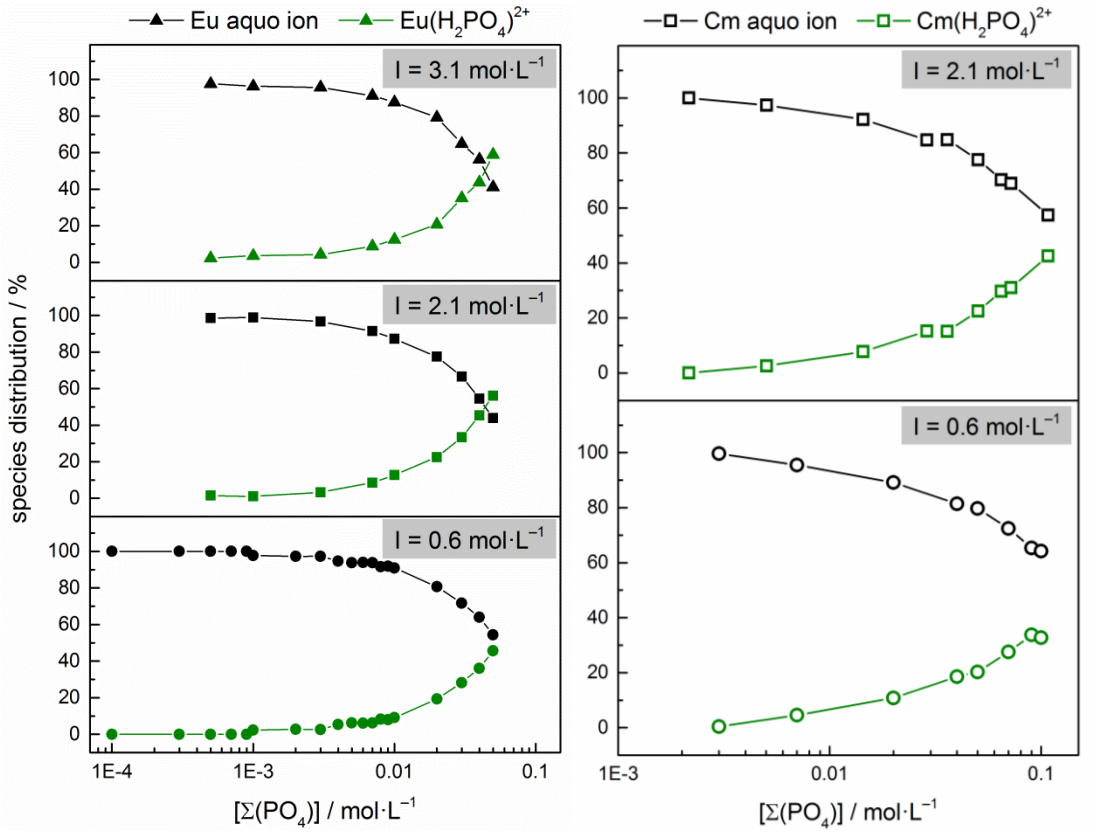

Figure S3. Derived species distributions for the different ionic strengths (excluding I = 1.1 mol·L^{-1} which is presented in the main text) for Eu(III) (left) and Cm(III) (right).

From these species distributions, slope analysis in the molal scale could be performed, Figure S4 and S5.

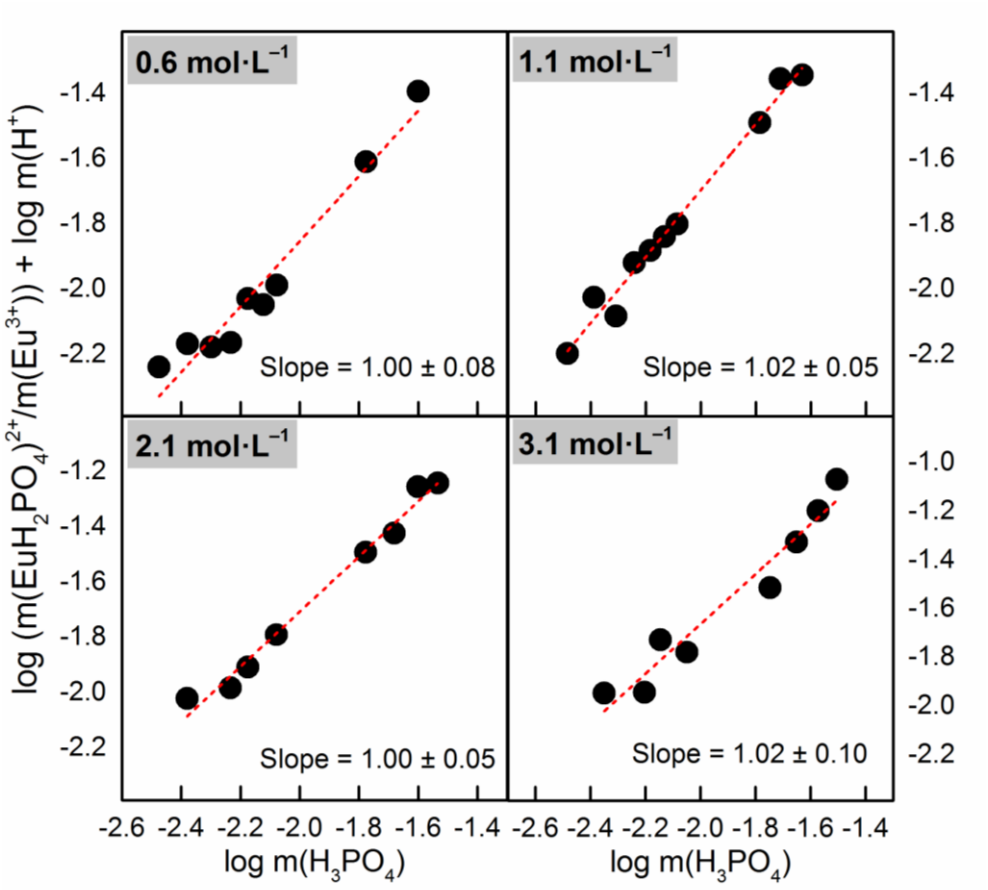

Figure S4. Slope analysis performed for the equilibrium $Eu^{3+} + H_3PO_4 \rightleftharpoons EuH_2PO_4^{2+} + H^+$ at 25 °C and for the different ionic strengths.

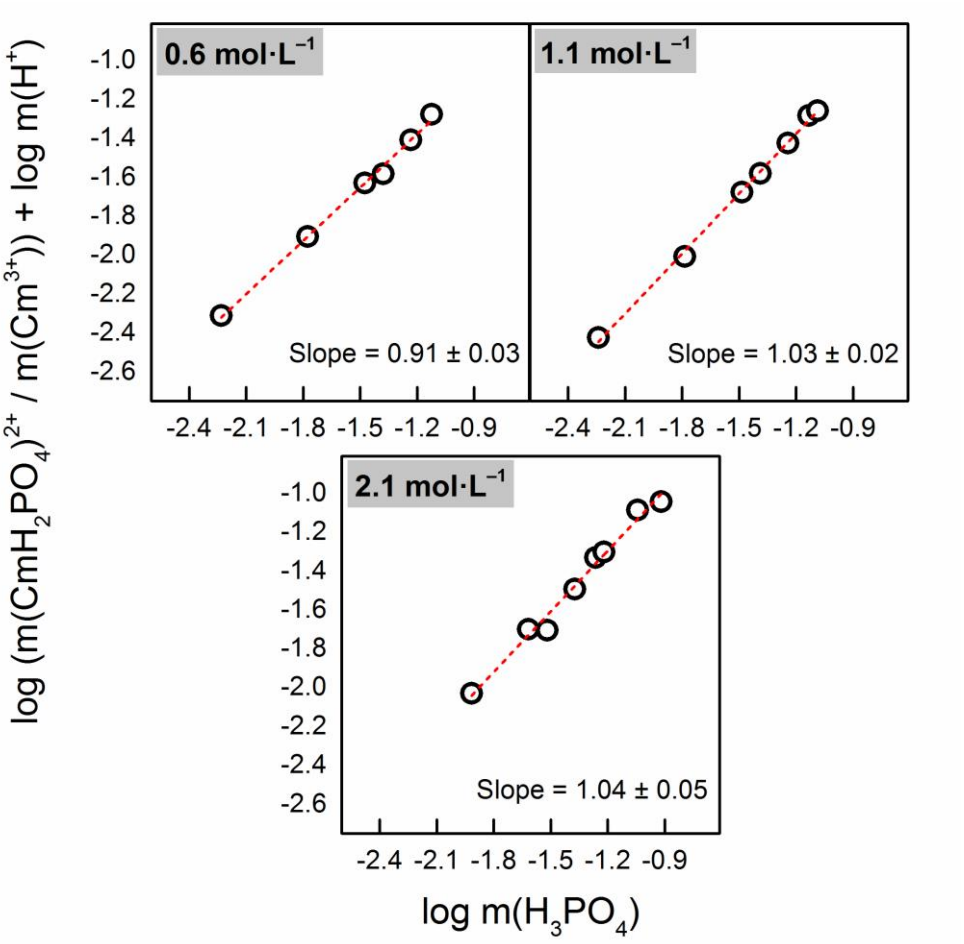

Figure S5. Slope analysis performed for the equilibrium $Cm^{3+} + H_3PO_4 \rightleftharpoons CmH_2PO_4^{2+} + H^+$ at 25 °C and for the different ionic strengths.

Laser spectroscopic investigations at I = 1.1 mol·L^{-1}, T = 40 °C and 60 °C

Selected emission spectra collected at 40 °C and 60 °C for Eu(III) and Cm(III) are presented in Figure S6.

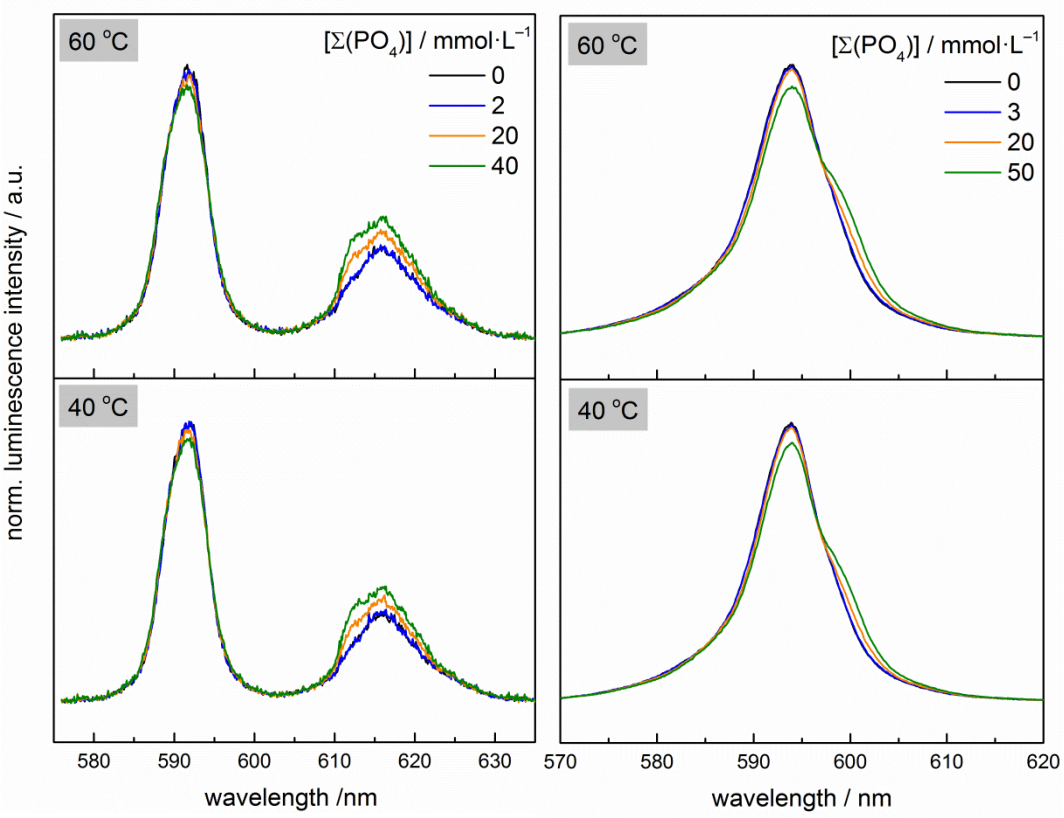

Figure S6. Selected emission spectra collected at 40 °C and 60 °C for Eu(III) (left) and Cm(III) (right). The spectra are normalized to the same $^7F_1$-band intensity in case of Eu(III) and the same total surface area in case of Cm(III).

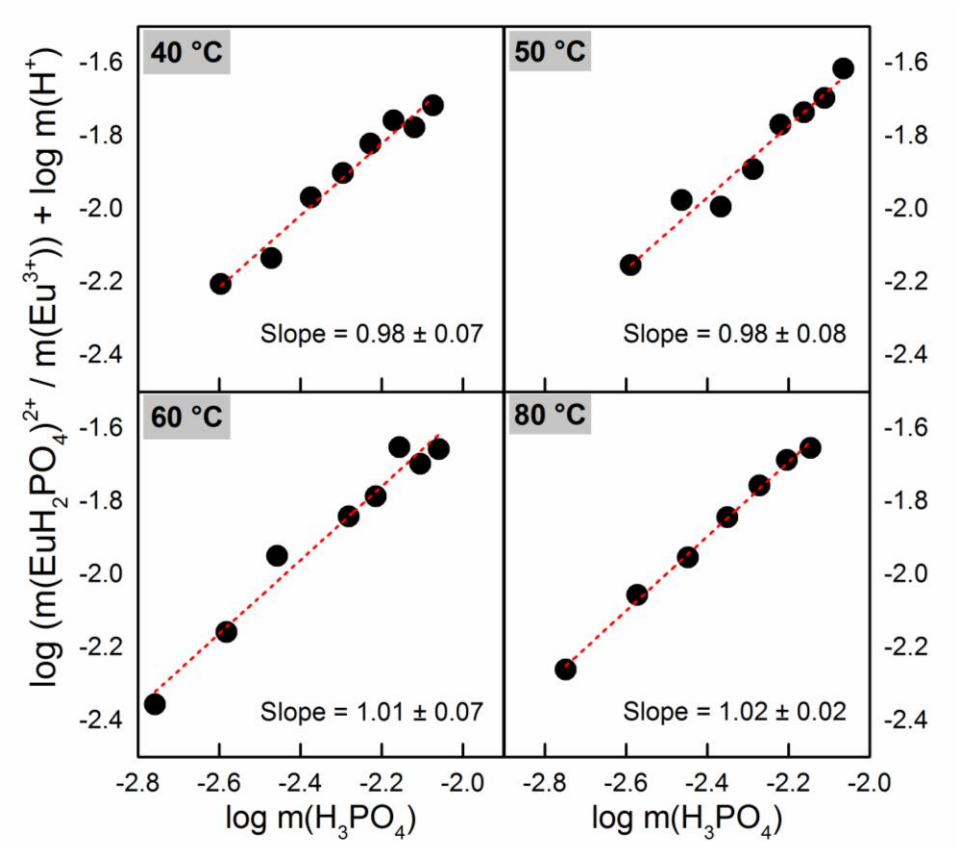

Figure S7. Slope analysis performed for the equilibrium $Eu^{3+} + H_3PO_4 \rightleftharpoons EuH_2PO_4^{2+} + H^+$ at elevated temperature and at I = 1.1 mol·L^{-1}.

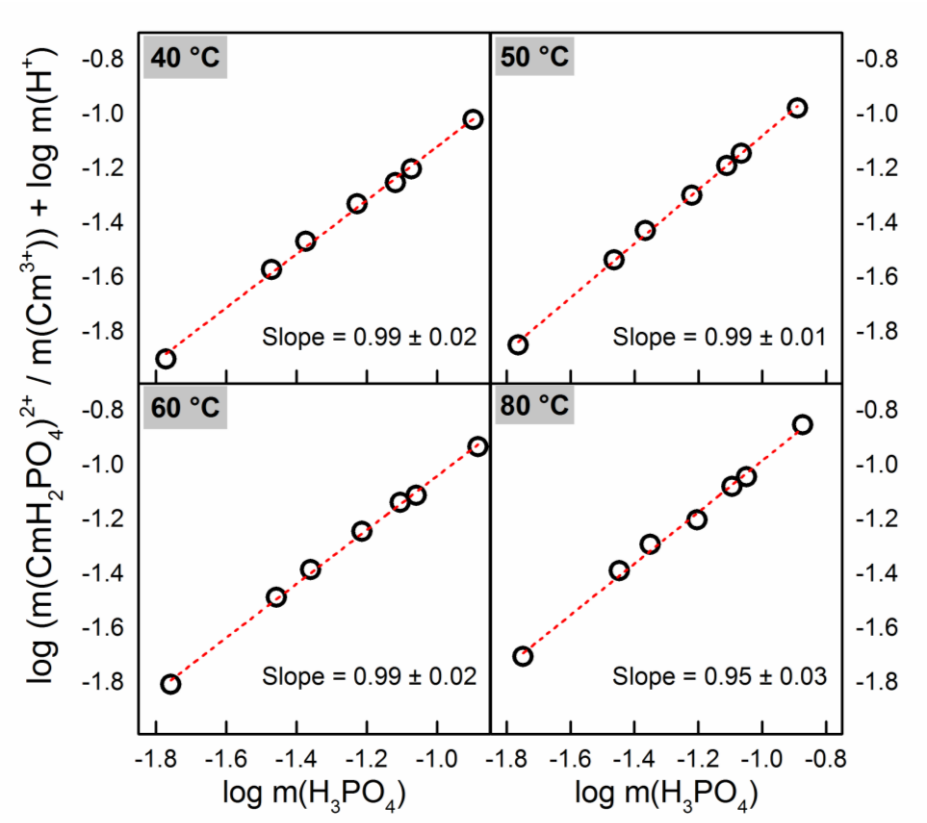

Figure S8. Slope analysis performed for the equilibrium $Cm^{3+} + H_3PO_4 \rightleftharpoons CmH_2PO_4^{2+} + H^+$ at elevated temperature and at I = 1.1 mol·L^{-1}.

Statistics for weighted linear regression

Statistical modelling in this paper follows a linear regression approach. The response variable is assumed to be a linear function of the input with added normal noise, i.e.

$$y_i = a + bx_i + \varepsilon_i, \qquad i = 1, \dots, n \tag{1}$$

Each error term is assumed to be uncorrelated with the other errors and normally distributed with mean 0 and an individual but known variance term: $\varepsilon_i \sim N(0, \sigma_i^2)$.

Parameter estimates for the regression line are obtained as the minimizers to the weighted least squares objective function

$$\sum_{i=1}^{n} w_i (y_i - a - bx_i)^2 \tag{2}$$

where weights are set to the reciprocal individual error variances $w_i = 1/\sigma_i^2$. This setting yields the best linear unbiased estimator for the regression parameters.[1]

Derivations of the results are best carried out using a linear algebra point of view to these equations and reformulating the model in matrix-vector notation as

$$y = F\beta + \varepsilon, \qquad Cov(\varepsilon) = diag(\sigma_1^2, \dots, \sigma_n^2) =: W^{-1} \tag{3}$$

with model matrix F consisting of two columns, the first containing only entries of 1, the second containing the values x_i and the parameter vector $\beta = (a, b)^T$.
Parameter estimates[1] are then given by $\hat{\beta} = (F^T W F)^{-1} F^T W y$ and predictions are obtained by $\hat{y} = F\hat{\beta}$.

From the assumption of normality of the errors it follows that the parameter estimates and therefore the predicted responses $\hat{y}$ are normally distributed as well with $\hat{y}_i \sim N(Ey_i,\ s_i^2)$ and $s_i^2 = (F(F^T W F)^{-1} F^T)_{i,i}$.

For the specific case of simple linear regression, the formulas turn out to be[2]:

$$\hat{a} = \frac{\left(\sum_{i=1}^{n} \frac{x_i^2}{\sigma_i^2}\right)\left(\sum_{i=1}^{n} \frac{y_i}{\sigma_i^2}\right) - \left(\sum_{i=1}^{n} \frac{x_i}{\sigma_i^2}\right)\left(\sum_{i=1}^{n} \frac{x_i y_i}{\sigma_i^2}\right)}{\Delta},$$

$$\hat{b} = \frac{\left(\sum_{i=1}^{n}\frac{1}{\sigma_i^2}\right)\left(\sum_{i=1}^{n}\frac{x_i y_i}{\sigma_i^2}\right)-\left(\sum_{i=1}^{n}\frac{x_i}{\sigma_i^2}\right)\left(\sum_{i=1}^{n}\frac{y_i}{\sigma_i^2}\right)}{\Delta},$$

$$\hat{y}_i = \hat{a} + \hat{b}x_i.$$

with Δ being defined as:

$$\Delta = \left(\sum_{i=1}^{n}\frac{1}{\sigma_i^2}\right)\left(\sum_{i=1}^{n}\frac{x_i^2}{\sigma_i^2}\right)-\left(\sum_{i=1}^{n}\frac{x_i}{\sigma_i^2}\right)^2$$

The standard deviations on $\hat{a}$ and $\hat{b}$ are then calculated based on[2]:

$$\sigma_{\hat{a}}^2 = \frac{1}{\Delta}\left(\sum_{i=1}^{n}\frac{x_i^2}{\sigma_i^2}\right)$$

and

$$\sigma_{\hat{b}}^2 = \frac{1}{\Delta}\left(\sum_{i=1}^{n}\frac{1}{\sigma_i^2}\right)$$

All computations were carried out with a script written in the R programming language.

References

1.Rencher, A. C.; Schaalje, G. B., *Linear models in statistics*. 2008.
2.Bevington, P. R.; Robinson, D. K., *Data reduction and error analysis for the physical sciences*. 1992.